Neurobiology of Aging 35 (2014) 2382–2393

Contents lists available at ScienceDirect

Neurobiology of Aging

journal homepage: www.elsevier.com/locate/neuaging

Age-related axonal swellings precede other neuropathological hallmarks in a knock-in mouse model of Huntington's disease☆

Martina Marangoni [a], Robert Adalbert [b], Lucie Janeckova [b,1], Jane Patrick [b,2], Jaskaren Kohli [a,3], Michael P. Coleman [b], Laura Conforti [a,*]

[a] School of Life Sciences, The University of Nottingham Medical School, Queen's Medical Centre, Nottingham, UK
[b] Babraham Institute, Babraham Research Campus, Cambridge, UK

ARTICLE INFO

Article history:
Received 28 November 2013
Received in revised form 20 April 2014
Accepted 23 April 2014
Available online 9 May 2014

Keywords:
Huntington's disease
Axon pathology
Yellow fluorescent protein
R6/2
HdhQ140
Stria terminalis
mHTT aggregates
Axonal swelling

ABSTRACT

Axon degeneration precedes cell body death in many age-related neurodegenerative disorders, often determining symptom onset and progression. A sensitive method for revealing axon pathology could indicate whether this is the case also in Huntington's disease (HD), a fatal, devastating neurodegenerative disorder causing progressive deterioration of both physical and mental abilities, and which brain region is affected first. We studied the spatio-temporal relationship between axon pathology, neuronal loss, and mutant Huntingtin aggregate formation in HD mouse models by crossing R6/2 transgenic and HdhQ140 knock-in mice with YFP-H mice expressing the yellow fluorescent protein in a subset of neurons. We found large axonal swellings developing age-dependently first in *stria terminalis* and then in cortico-striatal axons of HdhQ140 mice, whereas alterations of other neuronal compartments could not be detected. Although mutant Huntingtin accumulated with age in several brain areas, inclusions in the soma did not correlate with swelling of the corresponding axons. Axon abnormalities were not a prominent feature of the rapid progressive pathology of R6/2 mice. Our findings in mice genetically similar to HD patients suggest that axon pathology is an early event in HD and indicate the importance of further studies of *stria terminalis* axons in man.

1. Introduction

Huntington's disease (HD) is an age-related, devastating, autosomal dominant disorder caused by a CAG triplet expansion in the coding region of the Huntingtin gene (*IT15*). This results in an abnormal poly-glutamine (polyQ) stretch in the Huntingtin protein (HTT) (HDCRG, 1993) and manifests with progressive behavioral, cognitive and motor abnormalities, and inevitable early death. The main pathologic hallmark is the selective neurodegeneration of striatal medium sized spiny neurons, associated with extensive atrophy of the striatum (Ferrante et al., 1985; Graveland et al., 1985; Vonsattel et al., 1985). Other affected brain areas include cortical layers III and V, globus pallidus, and substantia nigra (Halliday et al., 1998; Vonsattel et al., 1985). Although striatal and cortical neuronal loss could underline the overt motor symptoms, earlier subtle behavioral changes and cognitive abnormalities, which precede motor symptoms by many years, might be better explained by neuronal dysfunction (Foroud et al., 1995; Lange et al., 1995; Lawrence et al., 1996; Mohr et al., 1991). Early studies on postmortem material from HD patients reported morphologic alterations in dendritic arbors and spines of medium sized spiny neurons, as well as in axons, by Golgi impregnation (Graveland et al., 1985) and immunostaining (Ferrante et al., 1991; Nihei and Kowall, 1992). Fiber density loss and reduction of fractional anisotropy, which is a measure of white matter integrity, have been observed in cortex and striatum of early stage HD patients (Reading et al., 2005; Weaver et al., 2009). Intranuclear (NIIs) and extranuclear (neuropil) aggregates of N-terminal mutant huntingtin fragments, produced by abnormal cleavage of the mutant form of HTT (mHTT), and a microscopic hallmark of HD, are also found to accumulate in dystrophic corticostriatal axons in patients (DiFiglia et al., 1997; Sapp et al., 1999). Nuclear inclusions could be toxic or represent an attempt by the cell to sequester soluble, more toxic forms of mHTT (Arrasate et al., 2004; Saudou

* Corresponding author at: School of Life Sciences, The University of Nottingham, Medical School, Queen's Medical Centre, Nottingham NG7 2UH, UK. Tel.: +44 115 8231476; fax: +44 115 823 0142.
E-mail address: Laura.Conforti@nottingham.ac.uk (L. Conforti).
[1] Present address: Antitope Ltd, Babraham Research Campus, Babraham, Cambridge CB22 3AT, UK.
[2] Present address: Wellcome Trust Sanger Institute, Wellcome Trust Genome Campus, Hinxton, Cambridge CB10 1SA, UK.
[3] Present address: St George's University of London, London SW170RE, UK.

0197-4580/$ – see front matter
http://dx.doi.org/10.1016/j.neurobiolaging.2014.04.024

et al., 1998). Instead, neuropil aggregates are generally associated with neuronal dysfunction (Chen et al., 2001; Davies et al., 1997; Gutekunst et al., 1999).

The study of the pathologic mechanisms underlining HD is facilitated by the availability of genetic mouse models, which reproduce some aspects of the human disease. In particular, transgenic (TG) R6/2 mice overexpressing a fragment of human mHTT (Mangiarini et al., 1996) are well characterized and widely used in preclinical studies. They show extensive atrophy of the striatum, cortex, and other brain regions as seen with histopathological techniques (Stack et al., 2005) and with MRI imaging (Sawiak et al., 2009), but little or no neuronal loss (Li and Li, 2004). They also show thinner dendrites, reduced dendritic spines (Klapstein et al., 2001), and early synapse dysfunction and loss, which may be the structural correlates of the development of cognitive dysfunction in the asymptomatic phase (Cepeda et al., 2003; Murphy et al., 2000). Electron microscopy studies established the presence of mHTT aggregates in axon terminals and a reduction of synaptic vesicles (Li et al., 2003). Knock-in (KI) mice are a genetically more precise HD model as they express the endogenous mouse HTT protein containing a human HTT N-terminal fragment with an expanded polyQ stretch (Menalled and Chesselet, 2002). They display some of the key features of the human disease with a milder phenotype and slower progression of the neuropathology compared with TG mice (Menalled, 2005). They show alterations in striatal synaptic activity (Usdin et al., 1999) and degenerative processes of the axons associated with the presence of mHTT neuropil aggregates (Li et al., 2001). In KI mice with 140 CAG repeats (HdhQ140 mice) (Menalled et al., 2003), reduction in striatal volume, dendrite complexity, and spine density alterations were reported (Lerner et al., 2012), followed by late neuronal loss (Hickey et al., 2008).

Early neurite dystrophies may be caused at least in part by defects in fast axonal transport, an essential process that delivers newly synthesized molecules from neuronal cell bodies to axons and synapses. Wild-type HTT plays an important role in fast axonal transport. It associates with vesicles and favors trafficking of synaptic proteins, organelles and signaling and trophic factors such as brain-derived neurotrophic factor (Gauthier et al., 2004). Instead, mHTT disrupts this process in different cellular and animal HD models (Gunawardena et al., 2003; Trushina et al., 2004), altering the normal transport of mitochondria (Orr et al., 2008), brain-derived neurotrophic factor (Wu et al., 2010), and synaptic vesicles and endosomes (Li et al., 2003). mHTT causes a disruption of JNK pathway and reduces kinesin-1 binding affinity to the microtubules (Morfini et al., 2006, 2009). Physical blockade of transport exerted by the aggregates has also been suggested in cultured striatal neurons (Li et al., 2001) and in *Drosophila* (Lee et al., 2004; Sinadinos et al., 2009).

Although this evidence suggests that axonal dysfunction contributes to HD pathology, it remains unclear in which neuronal compartment the first signs of degeneration occur and the spatial and temporal evolution of the degenerative changes. To address this question, we used yellow fluorescent protein (YFP)-H mice, which express the fluorescent marker protein YFP in a subset of neurons (Feng et al., 2000), as a tool to investigate axon pathology in HD models. We introduced the YFP-H transgene in R6/2 hemizygous (Mangiarini et al., 1996) and HdhQ140 heterozygous ($Hdh^{Q140/+}$) and homozygous ($Hdh^{Q140/Q140}$) mice (Menalled et al., 2003) and analyzed time-dependent alterations in the morphology of individual neuronal compartments, as previously reported in other models of neurodegeneration (Adalbert et al., 2009; Crowe and Ellis-Davies, 2013). In the HdhQ140 mice we detected an age-dependent formation of axonal swellings in the absence of significant changes in cell bodies, dendrites, and synapses. mHTT aggregate deposition paralleled the formation of axonal swellings but was topographically divergent. Interestingly, within the neuronal populations expressing YFP in our model, increased axonal swellings first appeared in the YFP positive axons of the *stria terminalis*, and only later in corticostriatal projections. In contrast, little or no disruption of axonal morphology was detected in R6/2/YFP-H mice where early synaptic abnormalities were found, in agreement with previous studies (Cepeda et al., 2003; Klapstein et al., 2001). Our results highlight important differences in the onset of pathology of distinct HD mouse models and may help explain some initial behavioral symptoms. The early axon pathology observed in *stria terminalis* in HdhQ140 mice underlines the importance of studying multiple brain areas in human patients, and the potential therapeutic value of understanding the mechanisms leading to axon degeneration in HD.

2. Methods

2.1. Mouse origins and breeding

Hemizygous R6/2 and homozygous HdhQ140 ($Hdh^{Q140/Q140}$) males (Mangiarini et al., 1996; Menalled et al., 2003) were bred to female Thy1.2-YFP-H homozygotes on a C57BL/6 background (Feng et al., 2000) to produce R6/2/YFP-H and heterozygous HdhQ140/YFP-H ($Hdh^{Q140/+}$/YFP-H) in the F1 generation. The latter were then intercrossed to produce mice homozygous for the Q140 mutation and hemizygous for YFP ($Hdh^{Q140/Q140}$/YFP-H). R6/2/YFP-H mice and YFP-H littermate controls aged 4- and 12-week-old were used, whereas HdhQ140/YFP-H and YFP-H littermates were used at 4 and 12 months for heterozygous and at 6 and 12 months for homozygous mice. All mice were obtained from The Jackson's laboratories (Bar Harbor, ME, USA) and kept at the Babraham Institute in Cambridge and at the University of Nottingham. All breeding and procedures were performed as authorized under the Animals (Scientific Procedures) Act 1986, under project licenses 80/2254, 40/3576, and 40/3482.

2.2. Genotyping

Tail tips or ear biopsies of 10-day-old mice were collected under isoflurane anesthesia. DNA was extracted from biopsies and genotyping was performed by polymerase chain reaction using the following forward (for) and reverse (rev) primers according to The Jackson's Laboratory Protocols (http://www.jax.org/):

R6/2

for: 5′- CCGCTCAGGTTCTGCTTTTA-3′
rev1: 5′-TGGAAGGACTTGAGGGACTC-3′
rev2: 5′-GGCTGAGGAAGCTGAGGAG-3′

HdhQ140

for1: 5′-CATTCATTGCCTTGCTGCTAAG-3′
rev1: 5′-CTGAAACGACTTGAGCGACTC-3′
for2: 5′-GATCGGCCATTGAACAAGATG-3′
rev2: 5′-AGAGCAGCCGATTGTCTGTTG-3′

For YFP genotyping, primers used were as follows:

for: 5′-CGAACTCCAGCAGGACCATGTGA-3′
rev: 5′-CTTCTTCAAGGACGACGGCAACT-3′

R6/2 and HdhQ140 DNA samples were sent to Laragen Inc (Culver City, CA, USA) for CAG repeat sizing.

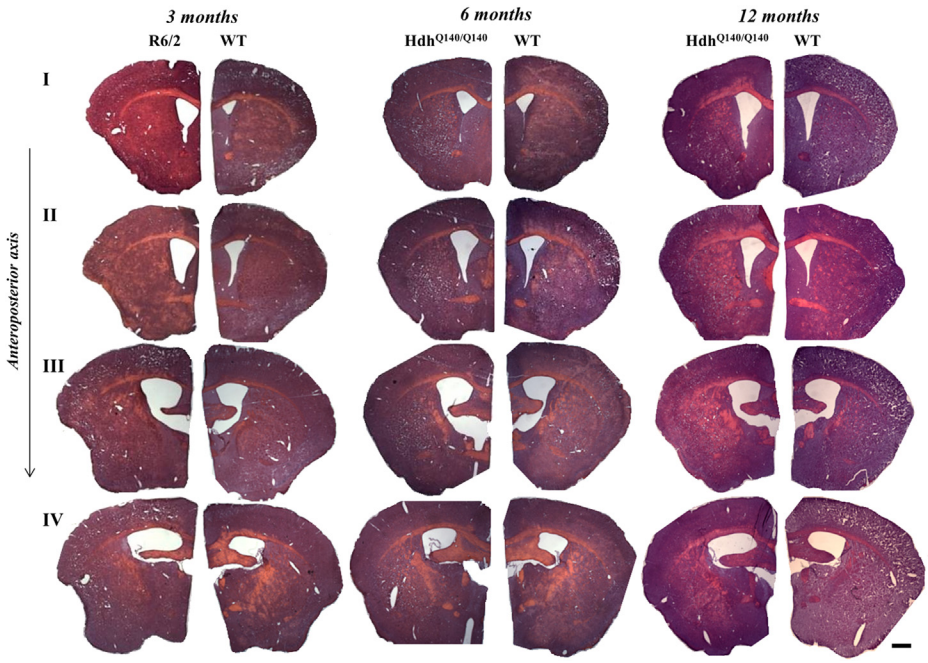

Fig. 1. HD mice show enlargement of the lateral ventricle. H&E stained coronal brain sections (20 μm) of 3-month-old R6/2/YFP-H and 6- and 12-month-old $Hdh^{Q140/Q140}$/YFP-H mice and corresponding YFP-H control littermates. Sections from 4 different anteroposterior brain levels were matched between HD and control mice and imaged (1.25×) for analysis of gross brain morphology (see Section 2). The area of the lateral ventricle was then measured for each section as described in Section 2. Representative sections from each genotype, brain level, and age are shown. Scale bar, 330 μm. See Table 1 for quantification. Abbreviations: HD, Huntington disease; YFP, yellow fluorescent protein.

2.3. Histology and immunohistochemistry

R6/2/YFP-H and HdhQ140/YFP-H mice, together with the corresponding YFP-H littermate controls, were perfused transcardially with 4% phosphate-buffered paraformaldehyde and brains dissected and processed as previously described (Adalbert et al., 2009). Brains were postfixed by overnight immersion in the same fixative and then cryoprotected in 30% sucrose at 4 °C for at least 48 hours before sectioning. Free-floating 50 μm sagittal and 20 μm coronal brain sections were later obtained using a Leica CM1850 cryostat. For evaluation of gross brain morphology, 20 μm coronal sections were mounted on Superfrost slides (BDH), air-dried and stained with Hematoxylin and Eosin (H&E) (Lillie, 1965). For morphologic analysis of YFP expressing (YFP+) neurons (Adalbert et al., 2009), 50 μm sagittal sections were incubated for 10 minutes with nuclear staining Hoechst 33258 diluted in phosphate-buffered saline (PBS) with 1% Triton (Invitrogen, 1:500), washed 3 times in PBS and then mounted onto Superfrost slides in Vectashield mounting medium (Vector Laboratories).

For immunohistochemistry, 20 μm coronal sections were incubated in PBS with 1% Triton for 10 minutes, washed 3 times in PBS and then blocked for 1 hour at room temperature (RT) with 3% BSA in PBS,

Table 1
Lateral ventricle areas were measured using Volocity 6.1 software in coronal brain sections of 4 different brain levels (I–IV) of 3-month-old R6/2 and 6- and 12-month-old $Hdh^{Q140/Q140}$ and corresponding control littermates

Age (mo)	Brain region (anteroposterior axis)	WT (n)(μm², mean ± SEM)	R6/2 (n)(μm², mean ± SEM)	HdhQ140/Q140 (n)(μm², mean ± SEM)
3	I	13 (293,072 ± 27,844)	13 (579573 ± 81,474)[a]	
	II	9 (526,545 ± 20,375)	9 (760,064 ± 59,105)[a]	
	III	6 (978,491 ± 79,757)	6 (1.367e+006 ± 99,906)[b]	
	IV	11 (756,578 ± 35,586)	11 (1.050e+006 ± 73,208)[a]	
6	I	10 (235,160 ± 29,300)		10 (401,635 ± 22,087)[a]
	II	9 (482,997 ± 62,436)		9 (853,790 ± 71,517)[a]
	III	9 (1.018e+006 ± 42,237)		9 (1.549e+006 ± 61,988)[c]
	IV	8 (657,449 ± 49,223)		8 (1.007e+006 ± 108,675)[b]
12	I	11 (373,382 ± 46,166)[d,e]		11 (489,113 ± 64,883)
	II	11 (839,953 ± 57,302)[e,f]		11 (851,451 ± 62,147)
	III	9 (1.282e+006 ± 31,097)[f,g]		9 (1.412e+006 ± 37,081)[b]
	IV	11 (743,956 ± 73,181)[d,e]		11 (1.034e+006 ± 91,635)[b]

A significant increase was found in all the 4 brain areas considered in R6/2 and $Hdh^{Q140/Q140}$ compared with control mice, at all time points (n = 3, mean ± SEM, unpaired Student t-test). A significant enlargement was also found within control mice at 12 months compared with 3 months (n = 3, mean ± SEM, 1-way ANOVA followed by Bonferroni post hoc test) and to 6 months (n = 3, mean ± SEM, 1-way ANOVA followed by Bonferroni post hoc test).
Key: ANOVA, analysis of variance; SEM, standard error of the mean; WT, wild type.
[a] $p < 0.01$.
[b] $p < 0.05$.
[c] $p < 0.001$.
[d] $p < 0.01$.
[e] $p < 0.001$.
[f] $p < 0.001$.
[g] $p < 0.01$.

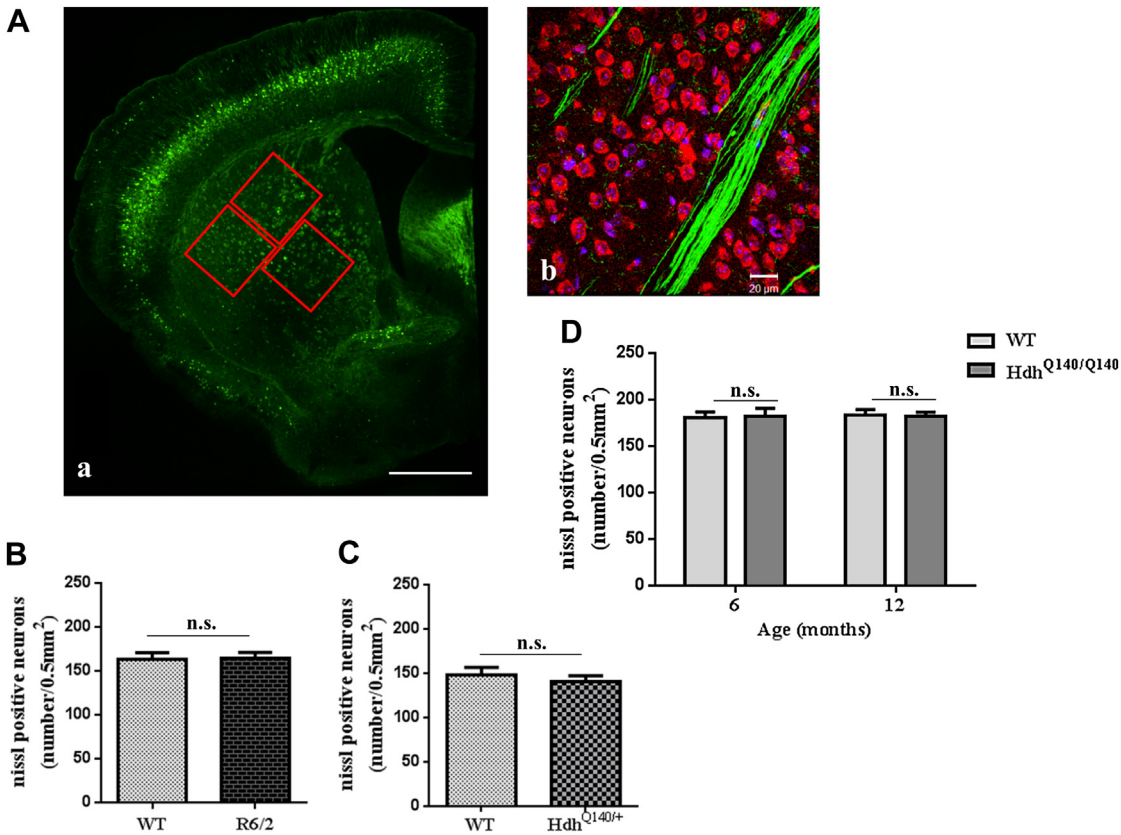

Fig. 2. The number of striatal neurons in HD mice is unaltered compared with controls. (A) The number of Nissl positive neurons was evaluated in coronal brain sections (20 µm) of HD/YFP-H mice and corresponding YFP-H control littermates. (a) Representative fluorescent image (2.5×) of a coronal brain section showing the 3 striatal fields (red boxes) acquired per each section for quantification of neuronal number (see Section 2). Scale bar, 100 µm. (b) Representative confocal image (40×) of a Nissl stained section corresponding to one of the fields quantified. Scale bar, 20 µm. Green: YFP, red: Nissl, blue: DAPI. (B–D) Quantitative analysis shows no significant cell loss in 3-month-old R6/2/YFP-H (B), 12-month-old $Hdh^{Q140/+}$/YFP-H (C), and 6- and 12-month-old $Hdh^{Q140/Q140}$/YFP-H (D) compared with the relative controls (n = 3–6, mean ± SEM, unpaired Student's *t* test and 1-way ANOVA followed by Bonferroni post hoc test). Abbreviations: ANOVA, analysis of variance; HD, Huntington disease; SEM, standard error of the mean; YFP, yellow fluorescent protein.

before overnight incubation at 4 °C with mouse anti-human huntingtin (Chemicon clone EM48, 1:100, Billerica, MA, USA). Goat anti-mouse Alexa Fluor 568 (Invitrogen, 1:200, Paisley, Scotland, UK) was used as secondary antibody (Adalbert et al., 2009). After incubation in secondary antibody, sections were mounted onto Superfrost slides in Vectashield mounting medium containing DAPI (Vector Laboratories).

To stain neuronal cell bodies, 20 µm coronal sections were incubated with NeuroTrace fluorescent Nissl stain in PBS (Invitrogen-Molecular Probes, 1:300; Peterborough, UK) in PBS for 20 minutes and then washed in PBS for 2 hours at room temperature before being mounted on slides in Vectashield containing DAPI.

2.4. Western blot

Western blot was carried out as previously described (Conforti et al., 2007). Fresh frozen striata and cortices from R6/2, HdhQ140, and wild-type littermate mice were homogenized in RIPA lysis buffer containing protease inhibitors (Complete mini, Roche; West Sussex, UK), protein samples loaded on a 10% SDS polyacrylamide gel, and then transferred to nitrocellulose membrane using a semi-dry blotting apparatus (BioRad; Hertfordshire, UK). Membranes were then blocked for 1 hour in 5% BSA in PBS plus 0.2% Tween-20 (PBST), incubated overnight with primary antibody in 5% BSA in PBST at 4 °C and subsequently incubated for 1 hour at RT with HPRT-linked secondary antibody in 2% BSA in PBST. The following primary antibodies were used: mouse anti-synaptophysin (Dako clone Y38, 1:10,000; Ely, UK) and mouse anti-PSD-95 (Abcam, 1:2000; Cambridge, UK). As loading control, mouse anti-β-tubulin III was used (Sigma, 1:5000; Gillingham, UK). Bands were visualized on film using a chemiluminescent detection kit (GE Healthcare; Amersham, UK).

2.5. Imaging and quantitative analysis

H&E stained sections were imaged by low power (Plan-NEOFLUOAR 1.25X/0.035) light microscopy (Zeiss Axioplan), and the area of the lateral ventricle was measured using Volocity 6.1 software. Sections representative of 4 different anteroposterior brain areas were matched between control and HD mice and used for the analysis.

For analysis of all fluorescently labeled sections, z-stack images were acquired by confocal microscopy (Zeiss LSM 710 Laser Scanning Microscope) at 1 airy unit with the following excitation/emission filters: DAPI/Hoechst 405 nm/420–480 nm, YFP 488 nm/505–550 nm, Alexa Fluor 568 and NeuroTrace 561 nm/575–615 nm. All quantitative analyses on confocal images were performed manually using ImageJ software, on maximum projection images resulting from the superimposition of the single z-stacks.

In particular, for morphologic characterization of YFP+ neurons and axons, confocal images were acquired with a 20× air-objective (Plan-Apochromat 20×/0.8) and axonal swellings quantified in 3 images per section, corresponding to cortex, striatum dorsal, and striatum ventral, in 3 sections per animal (n = 3–6, Fig. 3B). A cutoff of approximately 5 µm was used for swelling quantification and the analysis was carried out independently by 2 different persons, at least one of whom blinded to the mouse genotype (Bridge et al., 2009).

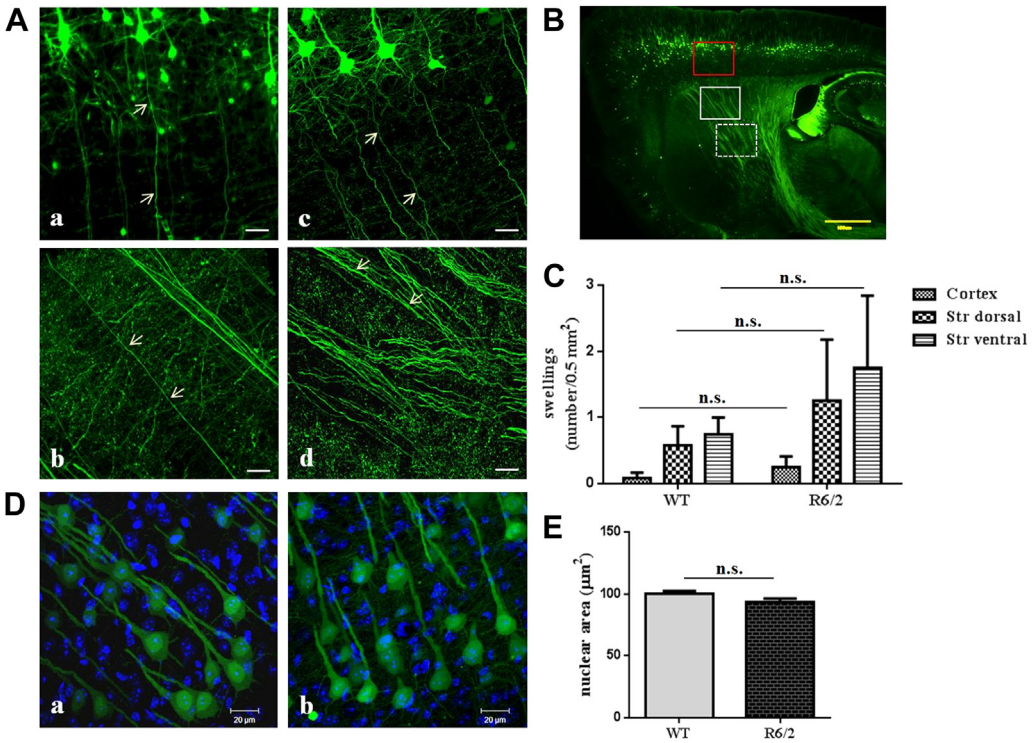

Fig. 3. R6/2 mice have normal cell bodies and no obvious axon abnormality. Sagittal brain sections (50 μm) of R6/2/YFP-H mice and corresponding YFP-H control littermates were imaged with confocal microscopy (20×) for analysis of axon morphology. (A) Mice aged 4- (a–b) and 12-week-old (c–d) show morphologically intact YFP+ neurons and projections both in cortex (a–c) and striatum (b–d). Arrows indicate continuous axonal tracts in cortex and striatum. Scale bar, 50 μm. (B–C) Quantification of the occasional swellings in cortex (red box), dorsal (white continuous box), and ventral (white-dashed box) striatum shows a tendency to an increase in R6/2/YFP-H mice compared with controls albeit with no significant difference (n = 4, mean ± SEM, 1-way ANOVA followed by Bonferroni post hoc test). Scale bar, 100 μm. (D) Confocal images (40×) of YFP+ cortical neurons of YFP-H (a) and R6/2/YFP-H (b) mice in sagittal brain sections stained with Hoechst show no gross morphologic changes in cell body morphology and (E) quantification of their nuclear size reveals no difference between the 2 genotypes (n = 4, mean ± SEM, unpaired Student's *t* test). Green: YFP, blue: Hoechst. Scale bar, 20 μm. Abbreviations: ANOVA, analysis of variance; SEM, standard error of the mean; YFP, yellow fluorescent protein.

For visualization and colocalization analysis of mHTT aggregates, confocal images were acquired using a 63× oil-immersion objective (Plan-Apochromat 63×/1.40). Colocalization studies were performed using Volocity 6.1 software, which allows 3D reconstruction of maximum projection images.

For analysis of nuclear size of Hoechst stained 50 μm sagittal sections in cortex and amygdala, a 40× oil-immersion objective (Plan-Apochromat 40×/1.3) was used and quantification was performed in 3 different brain sections per animal (n = 4–6). In the amygdala, a 0.035 mm^2 box was randomly placed within the imaged section and size of Hoechst stained nuclei of YFP+ cell bodies was measured within it (Adalbert et al., 2009).

Nissl stained sections were imaged at 40× and the number of Nissl positive neurons was quantified in 3 different striatal fields per section, in 3 sections per animal (n = 4–6, Fig. 2A).

WB bands were analyzed using ImageJ gel analysis software. For each band, the relative density was measured and then the adjusted density value, referred to the β-tubulin III loading control for each sample, was calculated.

2.6. Statistical analysis

Analysis and graphs were obtained using Prism GraphPad 5.0 software. Data were analyzed using Student's *t* test for independent samples and 1-way analysis of variance followed by Bonferroni post hoc test for multiple comparison. Data were expressed as mean ± standard error of the mean and considered statistically significant when *p*-value was <0.05.

3. Results

3.1. R6/2 and HdhQ140 mouse brain shows an age-dependent enlargement of the lateral ventricle but no striatal neuronal loss

To assess neuropathology in our HD mice we first looked at gross alterations in brain morphology in H&E stained sections. We compared matching sections representative of 4 different anteroposterior brain levels. In YFP-H control mice, the area of the lateral ventricle in sections representative of all 4 levels increases during aging, becoming significantly larger at 12 months of age compared with 3 and 6 months. Instead, there is no difference between 3 and 6 months of age (Fig. 1 and Table 1). Consistent with previous studies describing brain atrophy in R6/2 (Aggarwal et al., 2012; Sawiak et al., 2009) and $Hdh^{Q140/Q140}$ mice (Lerner et al., 2012), our results showed a significant enlargement of the lateral ventricle in 3-month-old R6/2 and 6- and 12-month-old $Hdh^{Q140/Q140}$ mice compared with control littermates (Fig. 1 and Table 1).

To investigate whether this was because of neurodegeneration, we determined the number of neurons in sections of R6/2 and HdhQ140 mouse brain striatum stained with Nissl dye (Fig. 2). Although with differences to the human phenotype, the striatum of HD mouse models remains the brain area where most neuropathological hallmarks, such as deposition of mHTT aggregates, have been described (Davies et al., 1997; Hickey et al., 2008) and where any potential neurodegeneration is most likely to be detected. We counted the number of Nissl stained neurons in striatal sections of 12-week-old R6/2 (Fig. 2B), 12-month-old $Hdh^{Q140/+}$ (Fig. 2C), and 6- and 12-month-old $Hdh^{Q140/Q140}$ (Fig. 2D) mice and found no significant

reduction compared with their control littermates. These results are consistent with previous evidence that HD mouse models show little or no neuronal loss at least until very late time points (Davies et al., 1997; Hickey et al., 2008) and suggest that more subtle changes preceding cell death might account for brain atrophy. In support of this, dendritic and synaptic abnormalities have been reported in HD patients and mouse models (Nithianantharajah and Hannan, 2013).

3.2. Axon swelling is an early feature of $Hdh^{Q140/Q140}$ mice

We then analyzed the morphology of corticostriatal neurons and axons of R6/2 and HdhQ140 mice crossed with YFP-H mice. Because of the restricted expression of the fluorescent protein, the YFP-H mouse line allows longitudinal tracing of individual neurons running from the cortical layer V toward the striatum passing through the corpus callosum and therefore enables visualization of all structures of these neurons, from dendrites to cell bodies to the long projection axons (Adalbert et al., 2009).

We first analyzed brain sections of 4- and 12-week-old R6/2/YFP-H mice corresponding to early and late stages of the disease in this mouse model (Mangiarini et al., 1996). At both time points, most fluorescent axons of R6/2/YFP-H mice looked morphologically normal and did not show signs of degeneration such as swellings or spheroids, typical features of the central nervous system axonal dysfunction during normal aging and in many disorders (Bridge et al., 2009; Ferguson et al., 1997; Galvin et al., 1999; Tsai et al., 2004) (Fig. 3A). We found a limited number of swellings in both R6/2 and control mice within the YFP expressing neurons, with a non-significant trend to an increase in the R6/2 mice (Fig. 3B and C). Moreover, no significant reduction in nuclear size of YFP+ cortical neurons stained with Hoechst was detected in these mice suggesting that the health status of the cell bodies was good (Adalbert et al., 2009) (Fig. 3D and E).

Next, we analyzed brain sections of 4- and 12-month-old $Hdh^{Q140/+}$ mice corresponding to early and advanced stage in this model, which carries the mutation in the appropriate genomic and protein context

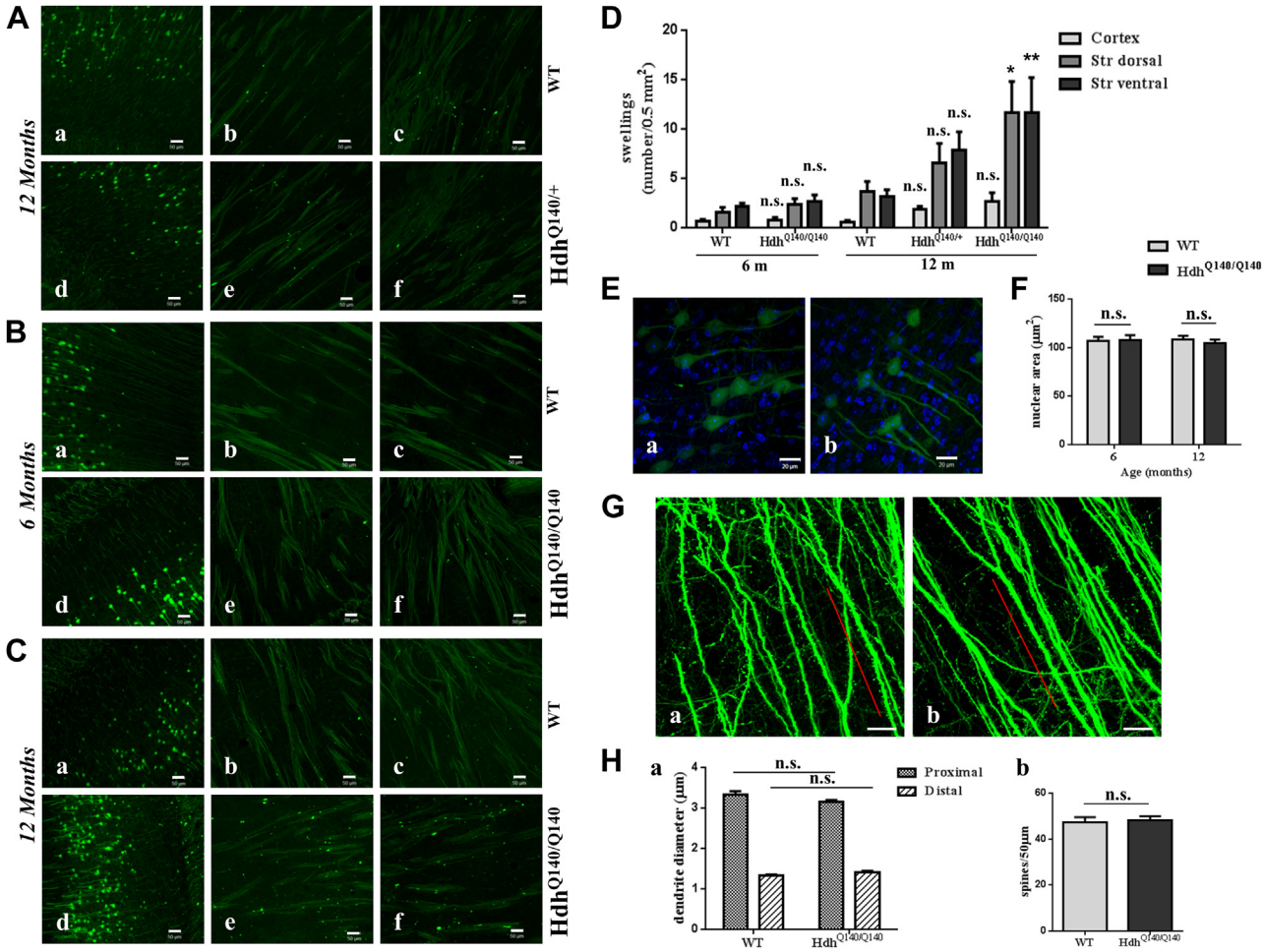

Fig. 4. Axonal swellings are detected in $Hdh^{Q140/Q140}$ mice before changes in cell bodies and dendrites. Confocal images (20×) of sagittal brain sections (50 μm) from (A) 12-month-old WT/YFP-H (a–c) and $Hdh^{Q140/+}$/YFP-H (d–f) mice, from (B) 6-month-old WT/YFP-H (a–c) and $Hdh^{Q140/Q140}$/YFP-H (d–f) mice and (C) 12-month-old WT/YFP-H (a–c) and $Hdh^{Q140/Q140}$/YFP-H (d–f) mice, show increased axonal swellings in the KI model compared with the controls. Scale bar, 50 μm. (D) Quantification of the number of swellings in cortex and striatum dorsal and ventral reveals a significant increase in the striatum of $Hdh^{Q140/Q140}$ mice compared with controls at 12 months of age. No difference could be detected in $Hdh^{Q140/Q140}$ at 6 months, whereas in $Hdh^{Q140/+}$ mice at 12 months we could detect a trend to an increase although it was not statistically significant (n = 3–6, mean ± SEM, 1-way ANOVA followed by Bonferroni post hoc test, * $p < 0.05$, ** $p < 0.01$, compared with the corresponding WT). (E) Confocal images (40×) of YFP+ neurons with nuclei stained with Hoechst in the cortex of (a) 12-month-old $Hdh^{Q140/Q140}$ and (b) control YFP-H mice show no gross morphologic changes. Scale bar, 20 μm. (F) Quantification of their nuclear areas did not show gross difference between the genotypes. (G) Dendrite morphology appears normal in 12-month-old $Hdh^{Q140/Q140}$ (a) compared with YFP-H control mice (b). (H) Quantification of (a) dendrite diameter and (b) spine density over 50 μm (red bar in G: a, b) shows no significant difference in $Hdh^{Q140/Q140}$ mice compared with YFP-H (n = 4, mean ± SEM, Student's *t* test). Scale bar, 20 μm. Green: YFP, blue: Hoechst. Abbreviations: ANOVA, analysis of variance; KI, knock in; SEM, standard error of the mean; WT, wild type; YFP, yellow fluorescent protein.

and at a heterozygous, physiological concentration. At 4 months we could not find any abnormalities in the KI model compared with control mice (not shown). However, interestingly we found an increase in the number of axonal swellings of $Hdh^{Q140/+}$/YFP-H mice compared with YFP-H wild-type mice at 12 months (Fig. 4A) albeit this increase did not reach a statistically significant value (Fig. 4D).

Therefore, to test whether increasing mutant *Hdh* gene dosage accentuates the axonal morphologic abnormalities we detected in the heterozygous HdhQ140 mice, we analyzed YFP expressing neurons of $Hdh^{Q140/Q140}$ mice at 6 and 12 months of age. Importantly, homozygotes retain the advantages of normal gene expression pattern, physiological expression level, and normal RNA splicing despite differing from human patients in having 2 mutant copies of the gene. At 6 months, the number of swellings in corticostriatal axons was not significantly different from that of the controls and generally lower than that found in 12-month-old heterozygotes (Fig. 4B and D). However, we observed a striking, highly significant increase in the number of axonal swellings in 12-month-old $Hdh^{Q140/Q140}$/YFP-H compared with that in YFP-H controls (Fig. 4C and D). Morphologic alterations appeared to be limited to the axonal compartment as the nuclear size of the YFP+ neurons remained unaltered (Fig. 4E and F) as well as their gross dendritic morphology (Fig. 4G and H).

A big increase in axonal swellings in $Hdh^{Q140/Q140}$/YFP-H mice was detected in axons running through the *stria terminalis*, a limbic forebrain structure located in the proximity of the striatum and the lateral ventricle. Neurons whose axons form this structure are also YFP+ in our HD/YFP-H mice (Porrero et al., 2010) (Fig. 5A). Upon quantification, the number of axonal swellings in this area in $Hdh^{Q140/Q140}$ mice resulted to be significantly increased compared with the control mice already at 6 months and was even greater at 12 months (Fig. 5B). The morphology of YFP+ cell bodies located in the amygdala, an area that contains the cell bodies of the axons running in *stria terminalis* (Fig. 5C), appeared generally normal and their nuclear size was not altered in HdhQ140 compared with wild-type mice (Fig. 5D); only occasionally we could detect some dysmorphic cell bodies in a few of the mice, irrespective of the genotype (data not shown).

Taken together, these results suggest that axon dystrophy precedes cell body and dendrite abnormalities in the HdhQ140 HD model. In addition, they suggest that the corticostriatal pathway may not be the first site of degeneration, which can instead originate in other brain areas. On the other hand, a different sequence of neuropathological events characterizes the R6/2 model in which significant axonal degeneration could not be detected.

3.3. mHTT inclusions do not correlate with axon pathology

Next, we asked whether axon abnormalities correlate with the deposition of mHTT aggregates in HD mouse models. First, we analyzed by confocal microscopy brain sections of R6/2 mice at 4 weeks of age stained with EM48, an antibody widely used to detect human mHTT in mouse models (Gutekunst et al., 1999). We confirmed the presence of widespread small NIIs and neuropil aggregates in cortex and striatum at this time point, in addition to nuclear diffused fluorescence (Fig. 6A, a, b and e). At 12 weeks, NIIs appeared as one single larger inclusion per nucleus (Fig. 6A, c, d and f). These findings are in agreement with an earlier study, which described the age-dependent deposition of NIIs in the cortex and the striatum of R6/2 mice (Davies et al., 1997). 3D reconstruction of confocal images confirmed colocalization between mHTT aggregates and some YFP+ neurons in our models (Fig. 7A and

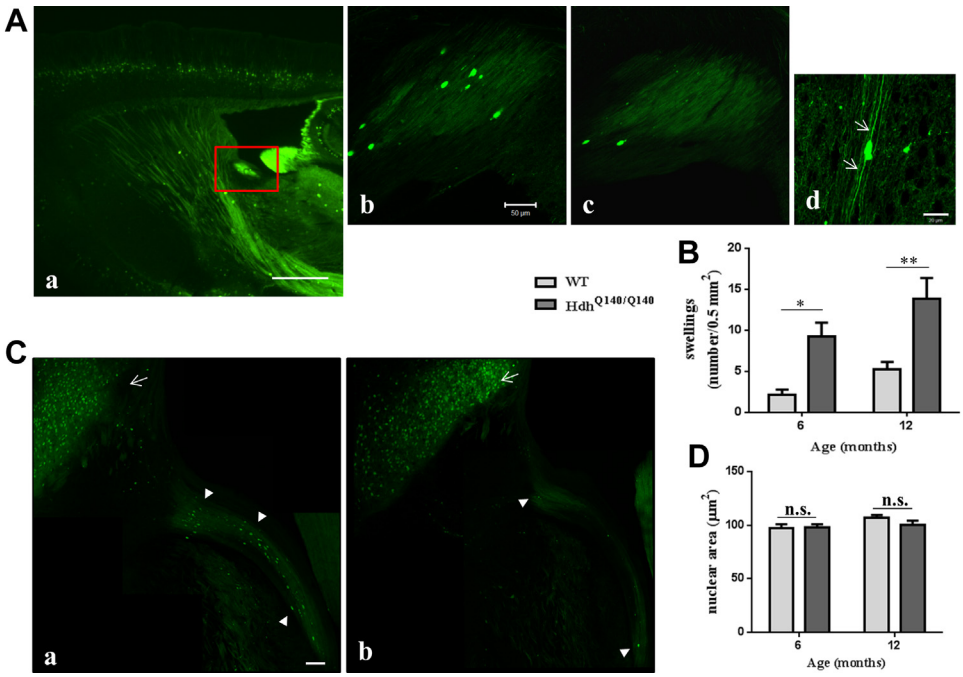

Fig. 5. Increased number of axonal swellings is detected in stria terminalis of $HdH^{Q140/Q140}$ mice. (A) Sagittal brain sections (50 µm) of $Hdh^{Q140/Q140}$/YFP-H and WT/YFP-H mice. (a) Representative fluorescent image (2.5×) of a sagittal brain section; the red box indicates the brain area of *stria terminalis* where a great number of axonal swellings was found. Scale bar, 100 µm. Images 20× of stria terminalis of (b) 6-month-old $Hdh^{Q140/Q140}$ and (c) control mice show increased swellings in the KI model compared with WT. Scale bar, 50 µm. (d) Higher magnification image reveals that axon continuity is maintained at both sides (white arrows) of the swelling. Scale bar, 20 µm. (B) Quantitative analysis of swellings in *stria terminalis* of $Hdh^{Q140/Q140}$ at 6 and 12 months of age shows significant increase compared with control mice. (C) Confocal reconstruction images of sagittal sections show a big number of axonal swellings in 12-month-old $Hdh^{Q140/Q140}$ mice (a) compared with control littermates (b) in axons running in the stria terminalis (white arrowheads). Their corresponding cell bodies are located in the amygdala (white arrows). Scale bar, 100 µm. (D) Quantification of the Hoechst stained nuclear area of YFP+ cell bodies in the amygdala reveals no significant difference between the genotypes (n = 4–5, mean ± SEM; 1-way ANOVA, * $p < 0.05$, ** $p < 0.01$). Abbreviations: ANOVA, analysis of variance; SEM, standard error of the mean; WT, wild type; YFP, yellow fluorescent protein.

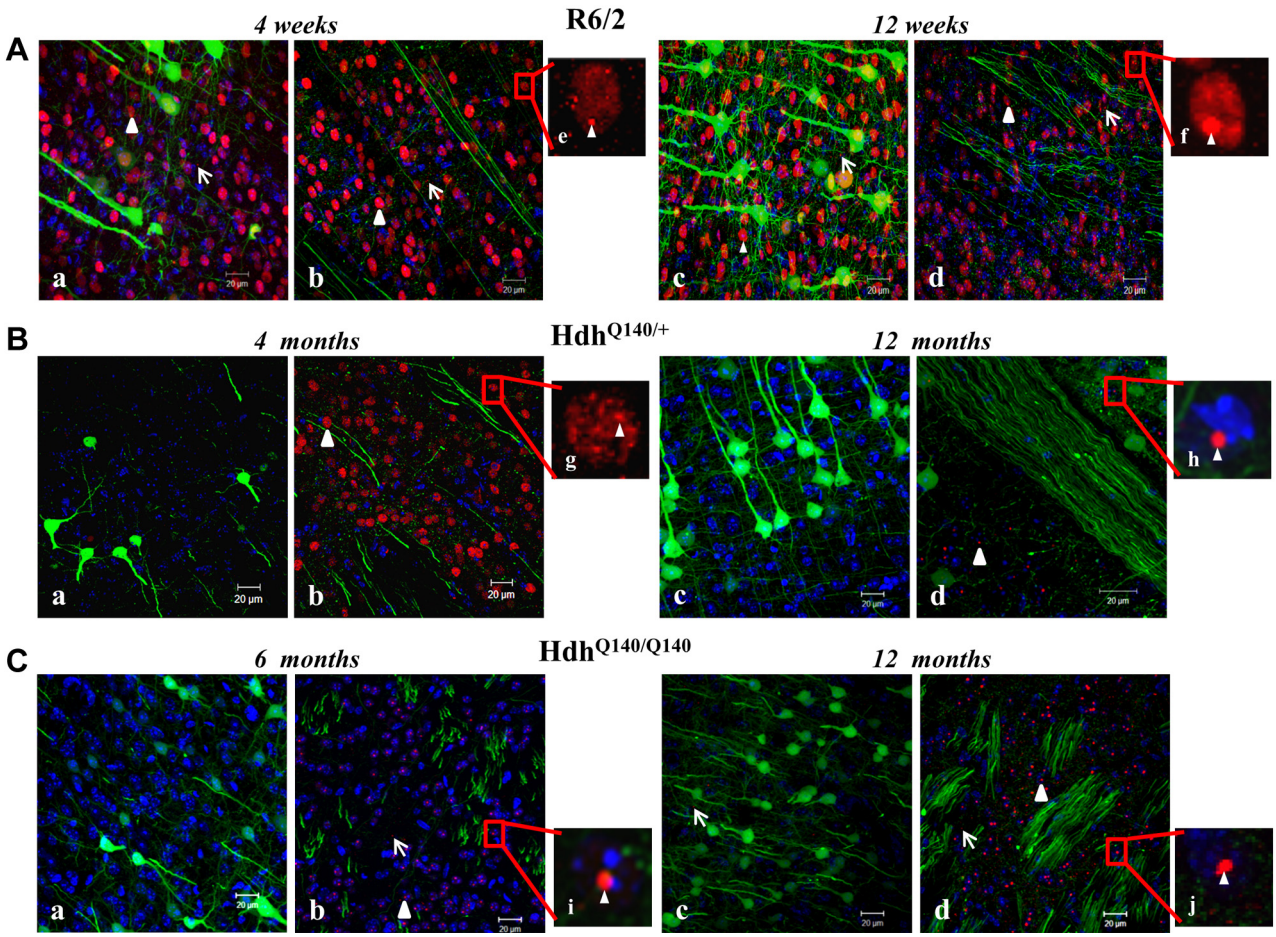

Fig. 6. Spatio-temporal characterization of mHTT aggregate formation in HD models. Coronal sections (20 μm) of R6/2/YFP-H and HdhQ140/YFP-H mice. Sections were immunostained with anti-HTT antibody (EM48) and imaged under high-resolution (63×) confocal microscopy to characterize mHTT inclusions. (A) R6/2 mice aged 4-week-old show small intranuclear (arrowhead) and extranuclear (arrow) mHTT aggregates both in (a) cortex and (b) striatum. R6/2/YFP-H mice aged 12-week-old show large intranuclear (arrowhead) and small extranuclear (arrow) mHTT aggregates both in (c) cortex and (d) striatum. Strong diffused nuclear staining is also visible. (B) $Hdh^{Q140/+}$/YFP-H mice aged 4-month-old show small intranuclear (arrowhead) mHTT aggregates in the (b) striatum although no immunostaining is detected in (a) the cortex. $Hdh^{Q140/+}$/YFP-H mice aged 12-month-old show a large intranuclear aggregate (arrowhead) in the (d) striatum, and no aggregates in (c) the cortex. (C) $Hdh^{Q140/Q140}$/YFP-H mice at 6 months of age show large intranuclear aggregates (arrowhead) in (b) the striatum and no staining in (a) the cortex. In 12-month-old $Hdh^{Q140/Q140}$/YFP-H mice small extranuclear aggregates appear in the cortex (c, arrow) in addition to the large NIIs detectable in striatum (d). (e–j) enlarged images from the corresponding boxed areas show mHTT aggregates in the nucleus (arrowheads). Scale bar, 20 μm. Green: YFP, red: mHTT, blue: DAPI. Abbreviations: HD, Huntington's disease; mHTT, mutant Huntingtin; YFP, yellow fluorescent protein.

Supplementary Video 1); however, we were unable to detect any colocalization between the small neuropil aggregates and the YFP+ axons with this imaging approach (Fig. 7B and Supplementary Video 2). Thus, neurons of R6/2 mice develop big mHTT intranuclear aggregates and yet maintain normal axon morphology.

In agreement with previous characterizations (Menalled et al., 2003), the deposition of mHTT aggregates follows a slower time course in HdhQ140 mice. In the striatum of $Hdh^{Q140/+}$ mice at 4 months of age only small NIIs were detected, whereas no immunostaining was visible in the cortex (Fig. 6B, a, b and g). At this time point, in contrast to the earlier description from Menalled et al. (2003), we could not clearly detect neuropil inclusions in striatum and cortex. At 12 months, striatal NIIs increased in size but still no immunoreactivity could be detected in the cortex (Fig. 6B, c, d and h).

In $Hdh^{Q140/Q140}$ mice at 6 months, large NIIs were detected in the striatum, whereas no immunoreactivity was present in the cortex, similar to heterozygotes at 12 months (Fig. 6C, a, b and i). In addition to the large NIIs in the striatum, small extranuclear aggregates appeared in the cortex of $Hdh^{Q140/Q140}$ mice at 12 months (Fig. 6C, c, d and j). Neither in the amygdala nor in the *stria terminalis*, could mHTT immunoreactivity be detected in homozygous KI mice (data not shown).

While these data confirm the subtle and progressive onset of mHTT deposition in our mouse models, they argue against a correlation between mHTT aggregates and the formation of axonal swellings. However, the presence and detrimental role of soluble mHTT in the abnormal axons cannot be excluded (Arrasate et al., 2004).

3.4. Synaptic abnormalities in HD mouse models

Synaptic transmission is altered in HD and abnormalities have been described at early time points in HD models (Smith et al., 2005). To investigate potential synaptic defects in our R6/2 and HdhQ140 mice and evaluate their temporal pattern of onset in relation to the axonal abnormalities, we looked at the expression levels of the presynaptic and postsynaptic marker proteins synaptophysin and PSD-95 by Western blotting.

In R6/2 mice at 12 weeks of age, a late time point in this mouse model but when axons still look intact (Fig. 3), the levels of both these synaptic markers appeared significantly reduced in the striatum, whereas no significant difference was found in the cortex (Fig. 8A and B).

Alterations in the level of neither synaptophysin nor PSD-95 were detected in cortex and striatum of $Hdh^{Q140/Q140}$ mice both at

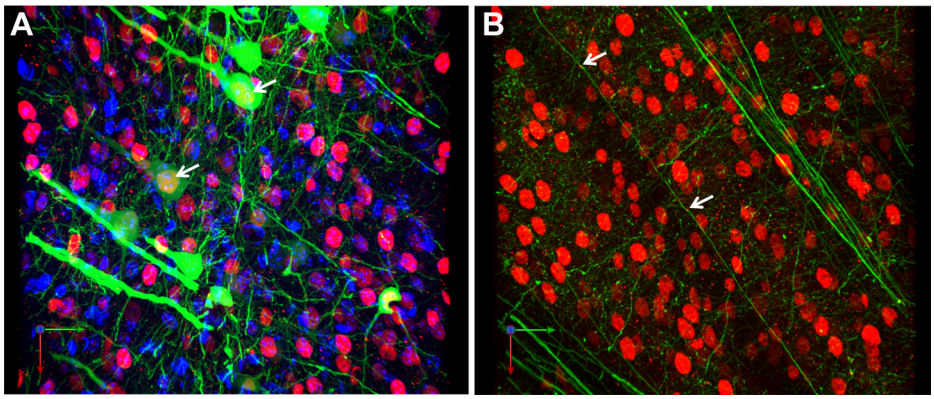

Fig. 7. (A) YFP+ neurons of R6/2 mice accumulate mHTT nuclear aggregates. Confocal images (63×) of coronal sections (20 μm) of 3-month-old R6/2/YFP-H mice immunostained with anti-HTT antibody (EM48). In the cortex, mHTT aggregates colocalize with the nucleus of YFP+ neurons (arrow) and this is confirmed by 3D reconstruction (Supplementary Video 1). (B) Neuropil mHTT aggregates do not colocalize with YFP+ axons in R6/2 mice. In the striatum, colocalization between mHTT neuropil aggregates and YFP+ axons is not confirmed by 3D reconstruction (Supplementary Video 2). Scale bar: 20 μm. Green: YFP, red: mHTT, blue: DAPI. Abbreviations: mHTT, mutant Huntingtin; YFP, yellow fluorescent protein.

6 and 12 months of age (Fig. 8C and D). The same result was found at 12 months in the hypothalamus, one of the main areas where the axons running in *stria terminalis* project their synapses (Fig. 8E).

Taken together, these results suggest synaptic dysfunction is a prominent feature of disease in R6/2 transgenic mice and this precedes degeneration of other neuronal compartments. However,

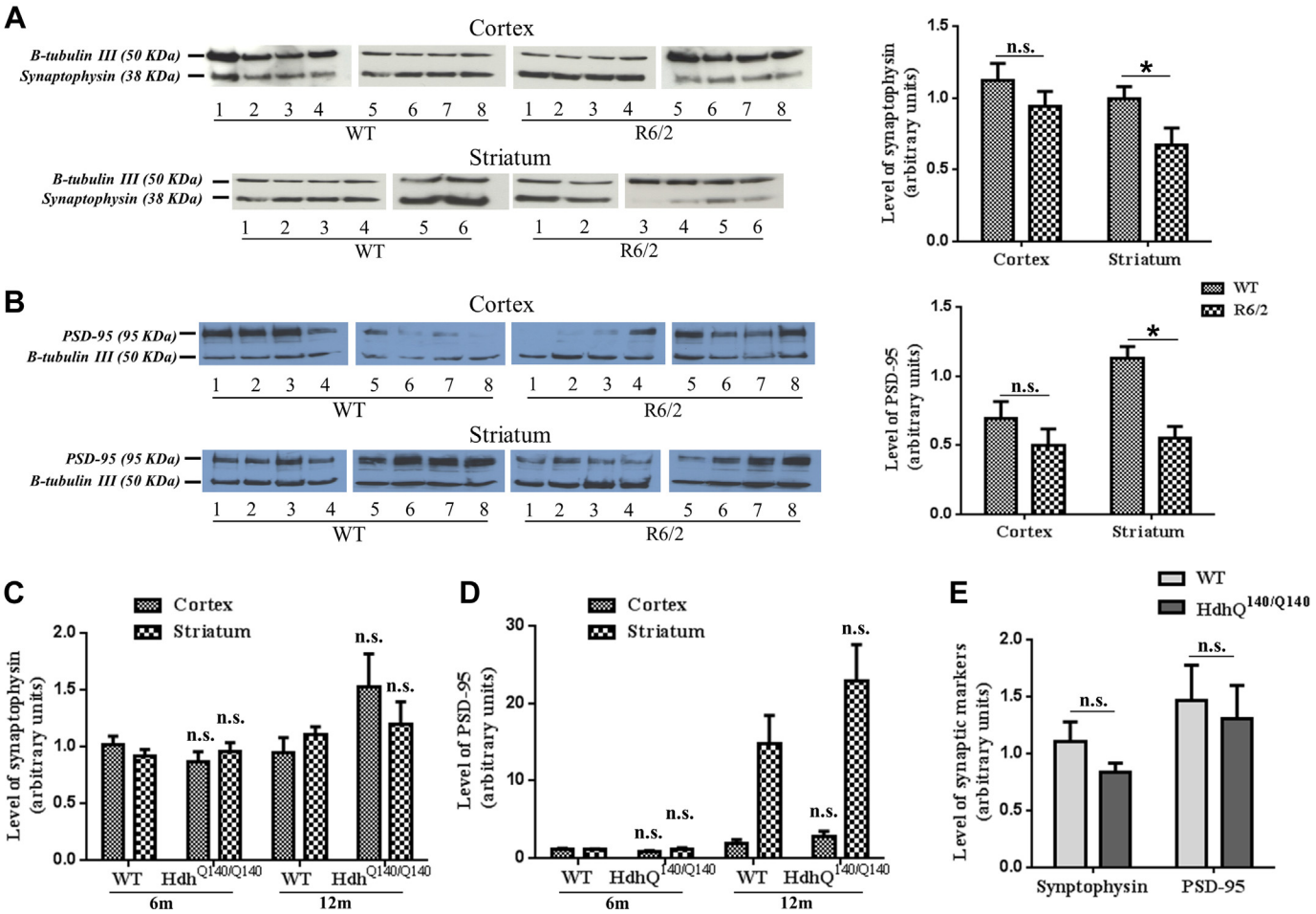

Fig. 8. Levels of synaptic markers in HD mouse brains. Western blots of mouse brain homogenates probed with antibodies against the presynaptic marker protein synaptophysin and PSD-95. β-tubulin III was used as a loading control in all blots (KDa 50). Blots for (A) synaptophysin (KDa 38) and (B) PSD-95 (KDa 95) of cortical and striatal homogenates of 12-week-old R6/2 and WT mice and corresponding quantification (right) show no significant reduction of both markers in the cortex of 3-month-old R6/2 compared with WT mice. In striatum, the level of synaptophysin (A) and PSD-95 (B) are significantly reduced compared with WT mice (n = 8, unpaired Student t-test, * $p < 0.05$, mean ± SEM). In $Hdh^{Q140/Q140}$ mice at 6 and 12 months of age we found no significant difference in the levels of (C) synaptophysin and (D) PSD-95 (n = 7–8, 1-way ANOVA followed by Bonferroni post hoc test). (E) The levels of synaptic markers in the hypothalamus of 12-month-old $Hdh^{Q140/Q140}$ mice do not differ from those of control littermates (n = 7–8, 1-way ANOVA followed by Bonferroni post hoc test). Abbreviations: ANOVA, analysis of variance; HD, Huntington's disease; SEM, standard error of the mean; WT, wild type.

in HdhQ140 KI mice, the level of synaptic markers are not altered at a time when axonal abnormalities are evident, suggesting that the sequence of neuropathological events can vary depending on the genetic model.

4. Discussion

The spatio-temporal evolution of axon pathology in HD patients and mouse models is still not well defined but its elucidation is important to focus the attention on appropriate therapeutic approaches. Our results suggest that axon degeneration precedes death of other neuronal compartments in a model of HD genetically similar to HD patients and could initiate in brain areas which have not been described as primary site of pathology in HD.

In $Hdh^{Q140/Q140}$/YFP-H mice we found a striking increase in the number of axonal swellings compared with YFP-H mice at 6 and 12 months of age, preceding cell body, dendrite, and synapse degeneration. Interestingly, axon pathology in this model was detected first in the *stria terminalis*, a brain area which is a part of the limbic system and plays a role in fear and anxiety related behavior. This structure, which is the first area to develop axonal swellings of those that could be visualized using this method, is not generally considered the primary site of degeneration in HD; however, recent studies have addressed the involvement of the limbic system in early behavioral symptoms in HD patients (Petersen and Gabery, 2012) and mice (Van Raamsdonk et al., 2005). A recent study describes early-onset defects suggestive of increased anxiety in HdhQ140 mice (Hickey et al., 2008), consistent with our findings that degenerative processes in axons are ongoing in this area. Only at the later time point of 12 months significant axon pathology extends to the corticostriatal axons of HdhQ140 mice. Axonal swellings in these mice are morphologically similar to those during normal aging but appear earlier and their number is significantly higher. Importantly, these morphologic abnormalities in HdhQ140 mouse axons seem to be independent of mHTT inclusion formation because no aggregate was detected in YFP+ neurons in the cortex and the amygdala, 2 areas where the cell bodies of corticostriatal axons and of *stria terminalis* axons are located. This suggests that other factors such as the presence of the toxic undetectable fraction of mHTT could play a role.

On the basis of our data, we propose that HdhQ140 mice, which allow the disease process to be studied in the context of an aging background, more similar to that in human patients, may represent a more accurate model to study axon degeneration during HD progression. Indeed, KI mice are genetically more similar to human HD patients; they have normal life span and milder phenotype resembling the presymptomatic stage of the disease in human patients. The combination of full-length mHTT expression at a physiological level, rather than just mutant N-terminal fragments as in transgenic models like the R6/2 mouse, and the slower progression of the disease which allows normal aging in these mice in parallel with disease onset, possibly explain the appearance of morphologic signs of axonal degeneration. Moreover, our results suggest that a certain level of mHTT is required to trigger axonal pathology as only homozygous HdhQ140 mice, and not heterozygotes, exhibit a significantly higher number of swellings compared with control mice at 1 year of age. In $Hdh^{Q140/+}$/YFP-H mice at 12 months, the increase in number of axonal swellings may be in part related to normal aging and potentially to YFP accumulation in aging animals rather than to HD pathology, as an increase with respect to earlier time points was observed both in KI mice and in control littermates with no statistically significant difference between the genotypes. This is consistent with previous observations suggesting that long-term expression of the YFP transgene itself increases age-related swellings in some axons (Bridge et al., 2009).

Our results in R6/2 mice confirm previous observations of synaptic abnormalities in the striatum of these mice (Cepeda et al., 2003; Klapstein et al., 2001) and we find they occur before cell body or axonal death. These abnormalities could result either by synaptic degeneration or by synaptic remodeling (Torres-Peraza et al., 2008). Conversely, axonal swelling and spheroid formation is not a prominent feature in these mice, nor is striatal neuronal death. These findings highlight some limitations of the transgenic model, which does not fully recapitulate the pathology of human HD. The aggressive phenotype with early death around 12–15 weeks of age makes the R6/2 mice particularly convenient for preclinical testing and therapy screening but less suitable for the investigation of the early mechanisms of an age-related disease that in human patients has late onset and slow progression.

YFP-H mice are a powerful tool to detect morphologic changes when crossed with neurodegenerative disease models and to assess axon pathology both in the central nervous system and peripheral nerves. Indeed, in a similar study on a mouse model of Alzheimer's disease (Adalbert et al., 2009), axonal swellings in the absence of any morphologic sign of cell body dysfunction was also observed. The similarities between our studies suggest analogies in the sequence of events leading to degeneration in these 2 different disease models.

In both HD models, we cannot exclude that axon degeneration occurs in non-YFP+ neurons. Striatal D_2 neurons, which are affected very early in HD progression (Albin et al., 1992; Reiner et al., 1988), are not fluorescently labeled in the YFP-H mouse line and we cannot rule out degeneration occurring in these neurons. Immunostaining with an anti-mHTT antibody in R6/2 mice revealed the presence of both intranuclear and neuropil mHTT aggregates but only the first were found to colocalize with YFP+ neurons. However, a colocalization and a toxic effect of neuropil aggregates on axons of non-YFP+ neurons cannot be excluded.

In conclusion, axon pathology was found in the HdhQ140 mouse as a primary event, which may initiate in brain areas other than those considered most susceptible to mHTT toxicity, whereas corticostriatal axons are affected at a later stage. Our results also underline important differences in the site where the first abnormalities are observed depending on the HD mouse model under study. Understanding the mechanism at the basis of axon pathology is likely to be crucial to alleviate symptom's onset and delay progression in HD.

Disclosure statement

The authors declare there are no actual or potential conflicts of interest.

Acknowledgements

The authors remember with affection Dr Terry Parker and they thank him for technical advice and helpful discussion. They also thank Tim Self for technical assistance with confocal microscopy and Jamie Webster for help with Western blotting. This work was funded by the CHDI Foundation (grant A-3255) (to Michael P Coleman and Laura Conforti), University of Nottingham Non clinical Senior Research Fellowship (to Laura Conforti), and University of Nottingham PhD studentship (to Martina Marangoni).

Appendix A. Supplementary data

Supplementary data associated with this article can be found, in the online version, at http://dx.doi.org/10.1016/j.neurobiolaging.2014.04.024.

References

Adalbert, R., Nogradi, A., Babetto, E., Janeckova, L., Walker, S.A., Kerschensteiner, M., Misgeld, T., Coleman, M.P., 2009. Severely dystrophic axons at amyloid plaques remain continuous and connected to viable cell bodies. Brain 132, 402–416.

Aggarwal, M., Duan, W., Hou, Z., Rakesh, N., Peng, Q., Ross, C.A., Miller, M.I., Mori, S., Zhang, J., 2012. Spatiotemporal mapping of brain atrophy in mouse models of Huntington's disease using longitudinal in vivo magnetic resonance imaging. Neuroimage 60, 2086–2095.

Albin, R.L., Reiner, A., Anderson, K.D., Dure, L.S., Handelin, B., Balfour, R., Whetsell Jr., W.O., Penney, J.B., Young, A.B., 1992. Preferential loss of striato-external pallidal projection neurons in presymptomatic Huntington's disease. Ann. Neurol. 31, 425–430.

Arrasate, M., Mitra, S., Schweitzer, E.S., Segal, M.R., Finkbeiner, S., 2004. Inclusion body formation reduces levels of mutant huntingtin and the risk of neuronal death. Nature 431, 805–810.

Bridge, K.E., Berg, N., Adalbert, R., Babetto, E., Dias, T., Spillantini, M.G., Ribchester, R.R., Coleman, M.P., 2009. Late onset distal axonal swelling in YFP-H transgenic mice. Neurobiol. Aging 30, 309–321.

Cepeda, C., Hurst, R.S., Calvert, C.R., Hernandez-Echeagaray, E., Nguyen, O.K., Jocoy, E., Christian, L.J., Ariano, M.A., Levine, M.S., 2003. Transient and progressive electrophysiological alterations in the corticostriatal pathway in a mouse model of Huntington's disease. J. Neurosci. 23, 961–969.

Chen, S., Berthelier, V., Yang, W., Wetzel, R., 2001. Polyglutamine aggregation behavior in vitro supports a recruitment mechanism of cytotoxicity. J. Mol. Biol. 311, 173–182.

Conforti, L., Fang, G., Beirowski, B., Wang, M.S., Sorci, L., Asress, S., Adalbert, R., Silva, A., Bridge, K., Huang, X.P., Magni, G., Glass, J.D., Coleman, M.P., 2007. NAD(+) and axon degeneration revisited: Nmnat1 cannot substitute for Wld(S) to delay Wallerian degeneration. Cell Death Differ 14, 116–127.

Crowe, S.E., Ellis-Davies, G.C., 2013. In vivo characterization of a bigenic fluorescent mouse model of Alzheimer's disease with neurodegeneration. J. Comp. Neurol. 521, Spc1.

Davies, S.W., Turmaine, M., Cozens, B.A., DiFiglia, M., Sharp, A.H., Ross, C.A., Scherzinger, E., Wanker, E.E., Mangiarini, L., Bates, G.P., 1997. Formation of neuronal intranuclear inclusions underlies the neurological dysfunction in mice transgenic for the HD mutation. Cell 90, 537–548.

DiFiglia, M., Sapp, E., Chase, K.O., Davies, S.W., Bates, G.P., Vonsattel, J.P., Aronin, N., 1997. Aggregation of huntingtin in neuronal intranuclear inclusions and dystrophic neurites in brain. Science 277, 1990–1993.

Feng, G., Mellor, R.H., Bernstein, M., Keller-Peck, C., Nguyen, Q.T., Wallace, M., Nerbonne, J.M., Lichtman, J.W., Sanes, J.R., 2000. Imaging neuronal subsets in transgenic mice expressing multiple spectral variants of GFP. Neuron 28, 41–51.

Ferguson, B., Matyszak, M.K., Esiri, M.M., Perry, V.H., 1997. Axonal damage in acute multiple sclerosis lesions. Brain 120 (Pt 3), 393–399.

Ferrante, R.J., Kowall, N.W., Beal, M.F., Richardson Jr., E.P., Bird, E.D., Martin, J.B., 1985. Selective sparing of a class of striatal neurons in Huntington's disease. Science 230, 561–563.

Ferrante, R.J., Kowall, N.W., Richardson Jr., E.P., 1991. Proliferative and degenerative changes in striatal spiny neurons in Huntington's disease: a combined study using the section-Golgi method and calbindin D28k immunocytochemistry. J. Neurosci. 11, 3877–3887.

Foroud, T., Siemers, E., Kleindorfer, D., Bill, D.J., Hodes, M.E., Norton, J.A., Conneally, P.M., Christian, J.C., 1995. Cognitive scores in carriers of Huntington's disease gene compared to noncarriers. Ann. Neurol. 37, 657–664.

Galvin, J.E., Uryu, K., Lee, V.M., Trojanowski, J.Q., 1999. Axon pathology in Parkinson's disease and Lewy body dementia hippocampus contains alpha-, beta-, and gamma-synuclein. Proc. Natl. Acad. Sci. U.S.A 96, 13450–13455.

Gauthier, L.R., Charrin, B.C., Borrell-Pages, M., Dompierre, J.P., Rangone, H., Cordelieres, F.P., De Mey, J., MacDonald, M.E., Lessmann, V., Humbert, S., Saudou, F., 2004. Huntingtin controls neurotrophic support and survival of neurons by enhancing BDNF vesicular transport along microtubules. Cell 118, 127–138.

Graveland, G.A., Williams, R.S., DiFiglia, M., 1985. Evidence for degenerative and regenerative changes in neostriatal spiny neurons in Huntington's disease. Science 227, 770–773.

Gunawardena, S., Her, L.S., Brusch, R.G., Laymon, R.A., Niesman, I.R., Gordesky-Gold, B., Sintasath, L., Bonini, N.M., Goldstein, L.S., 2003. Disruption of axonal transport by loss of huntingtin or expression of pathogenic polyQ proteins in Drosophila. Neuron 40, 25–40.

Gutekunst, C.A., Li, S.H., Yi, H., Mulroy, J.S., Kuemmerle, S., Jones, R., Rye, D., Ferrante, R.J., Hersch, S.M., Li, X.J., 1999. Nuclear and neuropil aggregates in Huntington's disease: relationship to neuropathology. J. Neurosci. 19, 2522–2534.

Halliday, G.M., McRitchie, D.A., Macdonald, V., Double, K.L., Trent, R.J., McCusker, E., 1998. Regional specificity of brain atrophy in Huntington's disease. Exp. Neurol. 154, 663–672.

HDCRG, 1993. A novel gene containing a trinucleotide repeat that is expanded and unstable on Huntington's disease chromosomes. Cell 72, 971–983.

Hickey, M.A., Kosmalska, A., Enayati, J., Cohen, R., Zeitlin, S., Levine, M.S., Chesselet, M.F., 2008. Extensive early motor and non-motor behavioral deficits are followed by striatal neuronal loss in knock-in Huntington's disease mice. Neuroscience 157, 280–295.

Klapstein, G.J., Fisher, R.S., Zanjani, H., Cepeda, C., Jokel, E.S., Chesselet, M.F., Levine, M.S., 2001. Electrophysiological and morphological changes in striatal spiny neurons in R6/2 Huntington's disease transgenic mice. J. Neurophysiol. 86, 2667–2677.

Lange, K.W., Sahakian, B.J., Quinn, N.P., Marsden, C.D., Robbins, T.W., 1995. Comparison of executive and visuospatial memory function in Huntington's disease and dementia of Alzheimer type matched for degree of dementia. J. Neurol. Neurosurg. Psychiatry 58, 598–606.

Lawrence, A.D., Sahakian, B.J., Hodges, J.R., Rosser, A.E., Lange, K.W., Robbins, T.W., 1996. Executive and mnemonic functions in early Huntington's disease. Brain 119 (Pt 5), 1633–1645.

Lee, W.C., Yoshihara, M., Littleton, J.T., 2004. Cytoplasmic aggregates trap polyglutamine-containing proteins and block axonal transport in a Drosophila model of Huntington's disease. Proc. Natl. Acad. Sci. U.S.A 101, 3224–3229.

Lerner, R.P., Trejo Martinez Ldel, C., Zhu, C., Chesselet, M.F., Hickey, M.A., 2012. Striatal atrophy and dendritic alterations in a knock-in mouse model of Huntington's disease. Brain Res. Bull. 87, 571–578.

Li, H., Li, S.H., Yu, Z.X., Shelbourne, P., Li, X.J., 2001. Huntingtin aggregate-associated axonal degeneration is an early pathological event in Huntington's disease mice. J. Neurosci. 21, 8473–8481.

Li, H., Wyman, T., Yu, Z.X., Li, S.H., Li, X.J., 2003. Abnormal association of mutant huntingtin with synaptic vesicles inhibits glutamate release. Hum. Mol. Genet. 12, 2021–2030.

Li, S.H., Li, X.J., 2004. Huntingtin and its role in neuronal degeneration. Neuroscientist 10, 467–475.

Lillie, R.D., 1965. Histopathologic Technic and Practical Histochemistry, third ed. McGraw-Hill Book Co, New York.

Mangiarini, L., Sathasivam, K., Seller, M., Cozens, B., Harper, A., Hetherington, C., Lawton, M., Trottier, Y., Lehrach, H., Davies, S.W., Bates, G.P., 1996. Exon 1 of the HD gene with an expanded CAG repeat is sufficient to cause a progressive neurological phenotype in transgenic mice. Cell 87, 493–506.

Menalled, L.B., 2005. Knock-in mouse models of Huntington's disease. NeuroRx 2, 465–470.

Menalled, L.B., Chesselet, M.F., 2002. Mouse models of Huntington's disease. Trends Pharmacol. Sci. 23, 32–39.

Menalled, L.B., Sison, J.D., Dragatsis, I., Zeitlin, S., Chesselet, M.F., 2003. Time course of early motor and neuropathological anomalies in a knock-in mouse model of Huntington's disease with 140 CAG repeats. J. Comp. Neurol. 465, 11–26.

Mohr, E., Brouwers, P., Claus, J.J., Mann, U.M., Fedio, P., Chase, T.N., 1991. Visuospatial cognition in Huntington's disease. Mov Disord. 6, 127–132.

Morfini, G., Pigino, G., Szebenyi, G., You, Y., Pollema, S., Brady, S.T., 2006. JNK mediates pathogenic effects of polyglutamine-expanded androgen receptor on fast axonal transport. Nat. Neurosci. 9, 907–916.

Morfini, G.A., You, Y.M., Pollema, S.L., Kaminska, A., Liu, K., Yoshioka, K., Bjorkblom, B., Coffey, E.T., Bagnato, C., Han, D., Huang, C.F., Banker, G., Pigino, G., Brady, S.T., 2009. Pathogenic huntingtin inhibits fast axonal transport by activating JNK3 and phosphorylating kinesin. Nat. Neurosci. 12, 864–871.

Murphy, K.P., Carter, R.J., Lione, L.A., Mangiarini, L., Mahal, A., Bates, G.P., Dunnett, S.B., Morton, A.J., 2000. Abnormal synaptic plasticity and impaired spatial cognition in mice transgenic for exon 1 of the human Huntington's disease mutation. J. Neurosci. 20, 5115–5123.

Nihei, K., Kowall, N.W., 1992. Neurofilament and neural cell adhesion molecule immunocytochemistry of Huntington's disease striatum. Ann. Neurol. 31, 59–63.

Nithianantharajah, J., Hannan, A.J., 2013. Dysregulation of synaptic proteins, dendritic spine abnormalities and pathological plasticity of synapses as experience-dependent mediators of cognitive and psychiatric symptoms in Huntington's disease. Neuroscience 251, 66–74.

Orr, A.L., Li, S., Wang, C.E., Li, H., Wang, J., Rong, J., Xu, X., Mastroberardino, P.G., Greenamyre, J.T., Li, X.J., 2008. N-terminal mutant huntingtin associates with mitochondria and impairs mitochondrial trafficking. J. Neurosci. 28, 2783–2792.

Petersen, A., Gabery, S., 2012. Hypothalamic and Limbic System Changes in Huntington's Disease. Journal of Huntington's Disease 1, 5–16.

Porrero, C., Rubio-Garrido, P., Avendano, C., Clasca, F., 2010. Mapping of fluorescent protein-expressing neurons and axon pathways in adult and developing Thy1-eYFP-H transgenic mice. Brain Res. 1345, 59–72.

Reading, S.A., Yassa, M.A., Bakker, A., Dziorny, A.C., Gourley, L.M., Yallapragada, V., Rosenblatt, A., Margolis, R.L., Aylward, E.H., Brandt, J., Mori, S., van Zijl, P., Bassett, S.S., Ross, C.A., 2005. Regional white matter change in pre-symptomatic Huntington's disease: a diffusion tensor imaging study. Psychiatry Res. 140, 55–62.

Reiner, A., Albin, R.L., Anderson, K.D., D'Amato, C.J., Penney, J.B., Young, A.B., 1988. Differential loss of striatal projection neurons in Huntington disease. Proc. Natl. Acad. Sci. U.S.A 85, 5733–5737.

Sapp, E., Penney, J., Young, A., Aronin, N., Vonsattel, J.P., DiFiglia, M., 1999. Axonal transport of N-terminal huntingtin suggests early pathology of

corticostriatal projections in Huntington disease. J. Neuropathol. Exp. Neurol. 58, 165–173.
Saudou, F., Finkbeiner, S., Devys, D., Greenberg, M.E., 1998. Huntingtin acts in the nucleus to induce apoptosis but death does not correlate with the formation of intranuclear inclusions. Cell 95, 55–66.
Sawiak, S.J., Wood, N.I., Williams, G.B., Morton, A.J., Carpenter, T.A., 2009. Use of magnetic resonance imaging for anatomical phenotyping of the R6/2 mouse model of Huntington's disease. Neurobiol. Dis. 33, 12–19.
Sinadinos, C., Burbidge-King, T., Soh, D., Thompson, L.M., Marsh, J.L., Wyttenbach, A., Mudher, A.K., 2009. Live axonal transport disruption by mutant huntingtin fragments in Drosophila motor neuron axons. Neurobiol. Dis. 34, 389–395.
Smith, R., Brundin, P., Li, J.Y., 2005. Synaptic dysfunction in Huntington's disease: a new perspective. Cell Mol. Life Sci. 62, 1901–1912.
Stack, E.C., Kubilus, J.K., Smith, K., Cormier, K., Del Signore, S.J., Guelin, E., Ryu, H., Hersch, S.M., Ferrante, R.J., 2005. Chronology of behavioral symptoms and neuropathological sequela in R6/2 Huntington's disease transgenic mice. J. Comp. Neurol. 490, 354–370.
Torres-Peraza, J.F., Giralt, A., Garcia-Martinez, J.M., Pedrosa, E., Canals, J.M., Alberch, J., 2008. Disruption of striatal glutamatergic transmission induced by mutant huntingtin involves remodeling of both postsynaptic density and NMDA receptor signaling. Neurobiol. Dis. 29, 409–421.
Trushina, E., Dyer, R.B., Badger 2nd, J.D., Ure, D., Eide, L., Tran, D.D., Vrieze, B.T., Legendre-Guillemin, V., McPherson, P.S., Mandavilli, B.S., Van Houten, B., Zeitlin, S., McNiven, M., Aebersold, R., Hayden, M., Parisi, J.E., Seeberg, E., Dragatsis, I., Doyle, K., Bender, A., Chacko, C., McMurray, C.T., 2004. Mutant huntingtin impairs axonal trafficking in mammalian neurons in vivo and in vitro. Mol. Cell Biol. 24, 8195–8209.
Tsai, J., Grutzendler, J., Duff, K., Gan, W.B., 2004. Fibrillar amyloid deposition leads to local synaptic abnormalities and breakage of neuronal branches. Nat. Neurosci. 7, 1181–1183.
Usdin, M.T., Shelbourne, P.F., Myers, R.M., Madison, D.V., 1999. Impaired synaptic plasticity in mice carrying the Huntington's disease mutation. Hum. Mol. Genet. 8, 839–846.
Van Raamsdonk, J.M., Pearson, J., Slow, E.J., Hossain, S.M., Leavitt, B.R., Hayden, M.R., 2005. Cognitive dysfunction precedes neuropathology and motor abnormalities in the YAC128 mouse model of Huntington's disease. J Neurosci 25, 4169–4180.
Vonsattel, J.P., Myers, R.H., Stevens, T.J., Ferrante, R.J., Bird, E.D., Richardson Jr., E.P., 1985. Neuropathological classification of Huntington's disease. J. Neuropathol. Exp. Neurol. 44, 559–577.
Weaver, K.E., Richards, T.L., Liang, O., Laurino, M.Y., Samii, A., Aylward, E.H., 2009. Longitudinal diffusion tensor imaging in Huntington's Disease. Exp. Neurol. 216, 525–529.
Wu, L.L., Fan, Y., Li, S., Li, X.J., Zhou, X.F., 2010. Huntingtin-associated protein-1 interacts with pro-brain-derived neurotrophic factor and mediates its transport and release. J. Biol. Chem. 285, 5614–5623.